JOURNAL OF GEOPHYSICAL RESEARCH, VOL. 102, NO. A12, PAGES 26,961-26,977, DECEMBER 1, 1997

Comparison of the high-latitude ionospheric electrodynamics inferred from global simulations and semiempirical models for the January 1992 GEM campaign

R. M. Winglee

Geophysics Program, University of Washington, Seattle

V. O. Papitashvili

Space Physics Research Laboratory, University of Michigan, Ann Arbor

D. R. Weimer

Mission Research Corporation, Nashua, New Hampshire

Abstract. The global characteristics of the auroral oval during the Geospace Environment Modeling (GEM) campaign of January 1992 are investigated through four different models: the assimilative mapping of ionospheric electrodynamics (AMIE) technique, the IZMIRAN electrodynamic model (IZMEM), the Weimer ionospheric convection model, and three-dimensional global fluid simulations. It is shown that all four models predict essentially the same key features with respect to the position, shape, and extent of the auroral convection cells, including the position of the separatrix between open and closed field lines. The relative change in the magnitude of the cross-polar cap potential is about the same for the different models, being between 20% and 50% in the case studies examined. However, there is some discrepancy by a factor of about 2 in predicting the absolute value. The global simulation potential is highest because it includes convection at low to middle latitudes, which appears to add about 50 kV to the total potential. It is shown that the auroral field-aligned currents are very sensitive to changes in B_z interplanetary magnetic field, with changes of the order of 200-300% in the total integrated current being inferred for the above changes in potential. The increase, particularly for the highest activity period, is due to an increase in the area of the oval rather than an increase in intensity.

1. Introduction

The characteristics of the auroral oval not only are important in themselves but they also provide an important means of remote sensing the dynamics of the magnetosphere. Remote sensing is aided by the fact that the region is continuously monitored by a large array of ground-based magnetometers and radars. In addition, the Defense Meterological Space Platforms (DMSP, F8-F11) provide frequent insitu observations at low altitudes. *Richmond and Kamide* [1988] developed the assimilative mapping of ionospheric electrodynamics (AMIE) technique that combines the above different data sets to produce synoptic maps of the auroral currents and potentials.

Paper number 97JA02461.
0148-0227/97/97JA-02461$09.00

The AMIE technique has been applied by *Lu et al.* [1995] and *Lyons et al.* [1996] to the Geospace Environment Modeling (GEM) campaign of January 27-28, 1992. This period was chosen because the interplanetary magnetic field (IMF) and solar wind conditions were approximately steady over durations of at least a couple of hours. Over such intervals each of the DMSP spacecraft can make two to three crossings of the auroral oval. In addition, the rotation of the earth increases the effective coverage of the oval by ground-based stations. This extensive coverage allows an important opportunity to quantify the latitudinal and magnetic local time (MLT) dependence of the field-aligned currents and electric potential and their relationship to the so-called separatrix that marks the boundary between open and closed field lines. *Lyons et al.* [1996] were able to show that during this period the cusp/mantle currents were on open field lines while the region 1 currents were on closed field lines. One of the features of the identified separatrix was that it often coincided

with a region of soft electron and magnetosheath-like ion precipitation (the soft electron zone).

Empirical models provide another important means for constructing synoptic maps of the cross-polar cap potential. One such empirical model is that of *Papitashvili et al.* [1994, 1995], which uses the fact that there appears to be a linear relationship between the interplanetary magnetic field (IMF) and disturbances observed by ground-based magnetometers. These coefficients have been determined empirically from archived magnetometer data and associated IMF conditions. The field-aligned current is inferred from the observed magnetic perturbations, and the cross-polar cap potential can then be calculated by using an assumed form for the ionospheric conductivity. This model is called the IZMIRAN Electrodynamic model (IZMEM), and the ionospheric conductivity assumed in the model takes into account differences in the dayside photoionization in the northern and southern hemispheres as the dipole tilt varies with season.

A different empirical model developed by *Weimer* [1995, 1996] uses the direct, double-probe measurements of the electric field from the DE 2. This model uses all such data during polar passes when IMF data were available from either ISEE 3 or IMP 8. The electric field data were then binned according to the B_y and B_z components of the IMF, and potential maps were constructed from the binned data.

The purpose of this paper is to compare results from three-dimensional (3-D) global fluid simulations with the results from AMIE, IZMEM, and Weimer models for the period covered by the GEM campaign of January 1992. The initial AMIE results for the campaign were published by *Lu et al.* [1995] and *Lyons et al.* [1996]. Each model has its strengths and weaknesses. The IZMEM and Weimer models can provide instantaneous predictions, while AMIE uses actual observed conditions. The global simulations provide an important means of treating the large-scale characteristics of the ionospheric currents and cross-polar cap potential in conjunction with the dynamics of the magnetosphere. The simulations also have the advantage that they can be used to investigate short-timescale processes such as substorm onset and magnetic reconnection in the magnetotail [*Winglee et al.*, 1997b]. The disadvantage of the global model is that most of the work to date has been on idealized cases studies and there are only a few published case studies of insitu comparisons, none of which make quantitative comparisons with observationally inferred field-aligned currents and potentials. By providing the four-way comparison in this paper one is better able to gain insight into persistent features in the auroral oval and their changes with solar wind conditions. In addition, one can also attain a better feel for the possible error estimates for the each of the models.

The details of the simulation model and the general properties of the solar wind conditions are described in section 2. The three case studies where there was extensive coverage of the oval are then discussed in subsequent sections. All three events were characterized by a strong dawnward component in the IMF (i.e., $B_y \lesssim$ -10 nT) and moderate dynamic pressure ($P_d \gtrsim 2$ nPa).

It is shown in section 3 that all four methods have important similarities including (1) the shape and positions of the currents and convection cells, (2) the position of the fastest convection, and (3) the position of the separatrix. However, there is a systematic difference in the estimated auroral potential with AMIE predicting the lowest value, followed in order by the Weimer model, IZMEM, and the global modeling. For the simulations, part of the difference is due to the fact that the strong B_y IMF greatly enhances the dusk (dawn) convection cell in the northern (southern) hemisphere such that there is still significant convection at midlatitudes on the dayside. Results from other global models [*Raeder*, 1997; *Slinker et al.*, 1997] indicate even higher (10-30 kV) potentials than those predicted by the present model.

All models show, for B_y IMF approximately constant at -20 nT and B_z IMF changing from +5 nT to -5 nT, that the cross-polar cap potential changes by only about 10-20% while the field-aligned currents into the ionosphere increase by 50-60%. As B_y IMF becomes less dawnward and B_z becomes more southward in the third event, similar percentage increases in the cross-polar cap potential and field-aligned currents occur. As a result there is a range of 20-50% in cross-polar cap potential and 200-300% in current. In the most active period, case 3, the increase in current comes from an increase in the area of the oval rather than an increase in the average current intensity. It is also shown that significant distortion of the *Iijima and Potemra* [1976, 1978] auroral currents can occur when B_y is the dominant component in the IMF.

2. Global Simulation Model

The fluid dynamics of a plasma are described by

$$\frac{\partial \rho}{\partial t} + \nabla \cdot (\rho \boldsymbol{V}) = 0 \tag{1}$$

$$\rho \frac{d\boldsymbol{V}}{dt} = -\nabla P + \boldsymbol{J} \times \boldsymbol{B} + \rho_q \boldsymbol{E} \tag{2}$$

$$\frac{\partial}{\partial t}\left(\frac{1}{2}\rho \boldsymbol{V}^2 + \frac{P}{(\gamma-1)}\right) + \nabla \cdot \left(\boldsymbol{V}\left(\frac{1}{2}\rho \boldsymbol{V}^2 + \frac{\gamma P}{(\gamma-1)}\right)\right) = \boldsymbol{J} \cdot \boldsymbol{E} \tag{3}$$

$$\frac{\partial \boldsymbol{B}}{\partial t} = -\nabla \times \boldsymbol{E}\,. \tag{4}$$

The space charge density ρ_q is given by

$$\nabla \cdot \boldsymbol{E} = \frac{\rho_q}{\epsilon_0} \tag{5}$$

and is in general small. It is most significant during reconnection where the $\boldsymbol{B}$ field can be small and the electric field large. Even under these conditions with the present resolution, the space charge term produces

at most only a few km/s corrections to the flow speeds. In more quiescent regions the correction is even smaller. However, in latter applications as grid resolutions are refined, it can become increasingly important. In addition, it is retained for self-consistency, so that when Ohm's law is subtracted from the momentum equation, the ion momentum equation is reproduced.

The other reason for retaining the space charge term is that it is used to calculate the magnetospheric potential, which is attained by inverting Poisson's equation,

$$\nabla^2\phi = -\frac{\rho_q}{\epsilon_0} . \tag{6}$$

This 3-D magnetospheric potential is calculated every 10 min of real time and an average is constructed over the observing period to facilitate comparisons with the other models which are using time-averaged data. The term magnetospheric potential is used here because it calculates the full potential being imposed across the magnetosphere. It includes all contributions from convection, including those at middle to low latitudes, and is not limited to just the high-latitude region. However, it does not include the field-aligned potential drops between the ionosphere and magnetosphere associated with the discrete aurora. These potential drops are due to kinetic effects at low altitudes and are not well incorporated in the global simulations. They can produce potential differences of several kV to possibly 10 to 20 kV during active periods.

To determine the cross-polar cap potential in conjunction with the values predicted by AMIE, IZMEM, and the Weimer empirical model, the magnetospheric potential is mapped down from near the simulation boundary onto the auroral region by using a simple dipole magnetic field. The 3-D potential can be affected by boundary conditions at the inner surface, for example, by mirror charges near conducting surfaces. In the calculation for the magnetospheric potential, (5) is used everywhere, so that the space charges inside the inner boundary are zero since the electric field is also zero there. To remove ambiguities the cross-polar cap potentials are constructed from the mapping of the magnetospheric potential at three grid points above the inner boundary. Test potentials constructed at two to five grid points away from the inner boundary showed essentially the same pattern and magnitude while the one at one grid point above the inner boundary had the same pattern but a magnitude half as small.

The fluid equations are closed by Ampere's law, which relates current to the magnetic field, usually approximated by $\boldsymbol{J} = \nabla \times \boldsymbol{B}$ and the generalized Ohm's law [e.g., *Krall and Trivelpiece*, 1986]. The generalized Ohm's law contains all the electron and ion dynamics including finite electron inertial effects and finite gyroradius effects. However, an exact solution of these equations requires a very small time step in order to resolve electron processes. Thus approximations for the generalized Ohm's law have to be made to attain a tractable solution.

Ideal MHD retains the two dominant terms of the generalized Ohm's law, i.e.,

$$\boldsymbol{E} + \boldsymbol{V} \times \boldsymbol{B} = 0 . \tag{7}$$

In this approximation the only electric field generated in the plasma is the convective electric field which is always orthogonal to $\boldsymbol{V}$ and $\boldsymbol{B}$. For this electric field the electrons and ions move as a single fluid under $\boldsymbol{E} \times \boldsymbol{B}$ drift motion. The configuration of the tail is such that the electric field lies essentially in the direction of the tail current, which is primarily in the y direction.

However, at the plasma sheet boundary layer there can be additional electric fields in the x and z plane [e.g., *Cattell and Mozer*, 1984]. In other words there can be significant electric fields near boundary layers that are not included in ideal MHD but which can have important effects on the the overall current system and convection. These processes can be included in part by assuming that the electrons with their high mobility are in approximate steady state equilibrium with the macroscopic electric and magnetic fields. In this case the electron momentum equation in steady state (i.e., $D\boldsymbol{V}_e/Dt = 0$) can be used to define the next higher order corrections to Ohm's law, i.e.

$$\boldsymbol{E} + \boldsymbol{V}_e \times \boldsymbol{B} + \frac{1}{en_e}\nabla P_e = 0 . \tag{8}$$

The ∇P_e term can produce corrections to the electric field in the plane orthogonal to the convective electric field $-\boldsymbol{V} \times \boldsymbol{B}$, as can differences in the bulk motion of the electrons $\boldsymbol{V}_e$ and the bulk plasma motion $\boldsymbol{V}$. In the presence of a nonuniform density, such as at boundary layers, these corrections can make contributions to the curl of the electric field, which in turn produces magnetic field and current perturbations. In the tail, for example, these perturbations can give rise to additional field-aligned currents in the x-z plane [*Winglee*, 1994] that divert current from the tail current sheet into the ionosphere. As a result of the resistance in the ionosphere this current diversion can produce an effective plasma resistivity on the tail current sheet that can be an important factor in determining the reconnection rate.

The electron momentum equation (8) can be cast into the more usual terms of an Ohm's law by noting that $\boldsymbol{J} = en(\boldsymbol{V}_i - \boldsymbol{V}_e)$ and $\boldsymbol{V} \simeq \boldsymbol{V}_i$. Making these substitutions into (6), we obtain the alternative form of the generalized Ohm's law where

$$\boldsymbol{E} + \boldsymbol{V} \times \boldsymbol{B} \simeq \left(\frac{\boldsymbol{J} \times \boldsymbol{B}}{en_e} - \frac{1}{en_e}\nabla P_e\right) . \tag{9}$$

In this form the $\boldsymbol{J} \times \boldsymbol{B}$ or Hall term comes from ion inertial/gyroradius effects in the sense that $\boldsymbol{V}_i \neq \boldsymbol{V}_e$. The Hall term acts much like the ∇P_e term to produce additional currents and electric fields that can be orthogonal to those of ideal MHD.

A perturbative solution was used by *Winglee* [1994] to show that the higher-order Ohm's law given by (9) can lead to additional field-aligned currents in the noon-midnight meridian and which map into the auroral re-

gion. This perturbative expansion is equally valid even in 3-D simulations. However, to avoid any ambiguities that arise from perturbative solutions, the following work is based on an exact solution to (9) with the assumption that the electron pressure P_e is equal to one half the total plasma pressure. This equipartition in temperatures is implicit in ideal MHD and is therefore an appropriate starting point to look at differences arising from nonideal MHD processes.

In the real magnetosphere there can be regions where the electron temperature can be much less than the ion temperature. The effect on the system in this case can be estimated by assuming that the ion fluid is in approximate equilibrium, i.e., $\boldsymbol{J} \times \boldsymbol{B} \simeq \nabla P$. In this case the right-hand side of (9) reduces to $(1/2)\boldsymbol{J} \times \boldsymbol{B}$ for equal electron and ion temperatures and to $\boldsymbol{J} \times \boldsymbol{B}$ when the electron temperature is much less than the ion temperature. This approximation is not made in the simulations but shows that the effects from the corrections to Ohm's law are still present even, when the electron temperature is relatively low.

In principle, the higher-order corrections in (9) can give rise to high-frequency/short-wavelength whistlers. These waves are not resolved in the present model (nor are they incorporated in MHD), and restrictions that they might impose on the time step and spatial scales do not appear to be relevant. Comparison with insitu measurements with Geotail and IMP 8 show that the model is able to produce reasonable agreement with observed magnetic fields in a variety of regions of the magnetosphere [*Winglee et al.*, 1997a].

The above equations are solved with a two-step Lax-Wendroff differencing scheme [*Richtmyer and Morton*, 1967] with a flux-correction smoothing scheme [*Boris and Book*, 1973]. The Lax-Wendroff scheme is one of the simpler methods for numerically solving partial differential equations. The advantage of this method is that it is robust and does not have to be modified as more physics is added to Ohm's law and the momentum equation. It is sometimes said that more sophisticated higher-order methods such as Riemann solvers (which have to break the perturbations into their different wave modes), offer less numerical dissipation than the Lax-Wendroff method. This statement is true for pure fluid applications, but it has recently been shown that because of the increased number of modes present in MHD its numerical dissipation rate is not significantly better than our chosen method [*Dongsu et al.*, 1995].

The simulations utilize a grid spacing in the near-Earth region of 0.7 R_E, which increases to about 3 R_E in the distant tail. While finer grid spacing is possible, it is not warranted in the present applications, as comparisons are being made with averages taken over several hours so that small scale processes are in general averaged out. The course resolution also provides saving in computer resources, so that the simulations can more easily cover the nearly 14 hours of real time involved in the three case studies. It is often assumed that because the above corrections to the ideal Ohm's law are proportional to the ion skin depth (c/ω_{pi}), they cannot be important at this resolution. In reality, the above nonideal effects have maximum strength and even dominate the convection term when the current sheet thickness reaches the ion skin depth, but their effects can be felt for current sheet thicknesses that are several times the ion skip depth, as in the present simulations.

The simulations extend 67 R_E on the flanks and 200 R_E into the tail. The inner radius of the simulations is set at 3.5 R_E, which is typical of most global simulations [e.g., *Ogino et al.*, 1994; *Fedder et al.*, 1995]. Around this inner boundary a resistive layer is incorporated that acts like the ionosphere. In this region the Ohm's law (7) is modified such that

$$\boldsymbol{E} + \boldsymbol{V} \times \boldsymbol{B} \simeq \left(\frac{\boldsymbol{J} \times \boldsymbol{B}}{en_e} - \frac{1}{en_e}\nabla P_e\right) + \eta_{iono}(r)\boldsymbol{J} \quad (10)$$

Note that while only a scalar resistivity is incorporated in (10), the actual conductivity is a tensor when the Hall term is combined with the resistivity term [cf. *Krall and Trivelpiece*, 1986]. By assuming that the magnitude of η_{iono} decreases rapidly with radial distance (in practice it is only significant within three cells of the inner radius) the Ohm's law allows a smooth transition from the collisional plasma of the ionosphere to the collisionless plasma of the magnetosphere. Placing the resistive layer inside the simulation system also has the advantage that the resistivity along the current path is not fixed, but rather can float, since the current can close at different altitudes depending on the forcing from the solar wind conditions.

The other feature of the ionospheric resistivity is that it is allowed to vary with both latitude and longitude consistent with (1) daylight ionization and (2) enhanced ionization from particle precipitation. For the daylight component the ion-neutral collision frequency (ν_{ni}) at the inner radius is assumed to equal the ion cyclotron frequency (Ω_i) at the equator and then to decrease to one tenth the value at the day-night terminator. The nightside collision frequency is assumed to be constant at one tenth the ion cyclotron frequency. Superimposed on this component, an additional component is centered at 65° magnetic latitude with a half width of 5°. The peak ion collision frequency arising from this component is also set at the ion cyclotron frequency. Note that in the limit $\nu_{ni}/\Omega_i \simeq 1$ the Hall conductivity reduces to $\sigma_H \simeq en_e/B$ as given in (10) which is about 5×10^{-5} mho/m on the dayside. The parallel or specific electrical conductivity has a minimum at the inner boundary of about 2×10^{-3} mho/m on the dayside and 2×10^{-2} on the dayside. Test experiments showed that doubling the resistivity could reduce the cross-polar cap potential by about 20%. No effort was made to adjust the assumed form of the conductivity to fit the inferred potential maps.

In addition, a dense (200 per cm^3) cold (3 eV) plasma representing the outer plasmaspheric population is loaded into the inner magnetosphere. The density of this component then falls off as $1/r^5$. This plasma, particularly in the resistive layer, in many ways acts like the iono-

sphere by providing a sink for energy flowing in from the magnetosphere. At the same time it provides a source of plasma that can be used to populate the tail, as is it shrinks and grows with activity. The motion of this plasma is determined by the convection induced by the solar wind interaction, but most of it remains on closed magnetic field lines. The inner boundary conditions are set at this density.

Test simulations with different density configurations indicate that the inclusion of this density component does not change the equilibrium attained by the magnetosphere, but it can change the timescale (of the order of 5 to 15 min). Since the relevant time period is several hours in the present application, the inclusion of the high-density component is not a limiting factor.

3. Case Studies

3.1. Solar Wind Conditions

The IMF conditions as observed by IMP 8 are shown in Figure 1. *Lyons et al.* [1996] divided the above period into four intervals when the IMF conditions were approximately steady : (1) January 27, 1520 UT $\pm$ 115 min with $\boldsymbol{B} \simeq (5, -20, 5)$ nT, (2) January 27, 1830 UT $\pm$ 60 min with $\boldsymbol{B} \simeq (5, -18, -4)$ nT, (3) January 28, 0115 UT $\pm$ 170 min with $\boldsymbol{B} \simeq (7, -13, -9)$ nT, and (4) January 28, 1905 UT $\pm$ 45 min with $\boldsymbol{B} \simeq (7, -3, 3)$ nT. The data for interval 4 were relatively sparse, and we have chosen not to include it here in order to limit the discussion.

The corresponding solar wind conditions are shown in Figure 2. For the 1830 and 0115 intervals the plasma conditions were also approximately constant with dynamic pressures of about 2.5 nPa and 4.4 nPa, respectively. However, for the first period the dynamic pressure increases from 2 to 5 nPa. To set up the simulations, they were first run for 2 hours with the solar wind conditions as observed at 1330 UT on January 27. This period sets up an approximately steady state magnetosphere consistent with the prevailing solar wind conditions. The simulations were then run continuously from 1330 UT on January 27 to 0400 UT on January 28. During the period of the data dropout between 1930 and 2100 UT the IMF conditions were simply interpolated between the known data points.

The B_x component of the IMF is incorporated into the simulations along with the B_y and B_z IMF components by adding the initial value of B_x IMF, in this case 5.0 nT, everywhere to the initial system; i.e., the initial magnetic field configuration consists of the terrestrial dipole plus a uniform component from the heliospheric current sheet. Temporal changes in B_x IMF are then incorporated by allowing the B_y and B_z components to have variations in y and z along the solar wind boundary. These variations are estimated by assuming that the solar wind field lines are straight with a direction vector (B_x, B_y, B_z), so that the distance to the solar wind boundary differs along the field line from the IMP 8 observing position. The corresponding time delay is then estimated by using the observed solar wind speed.

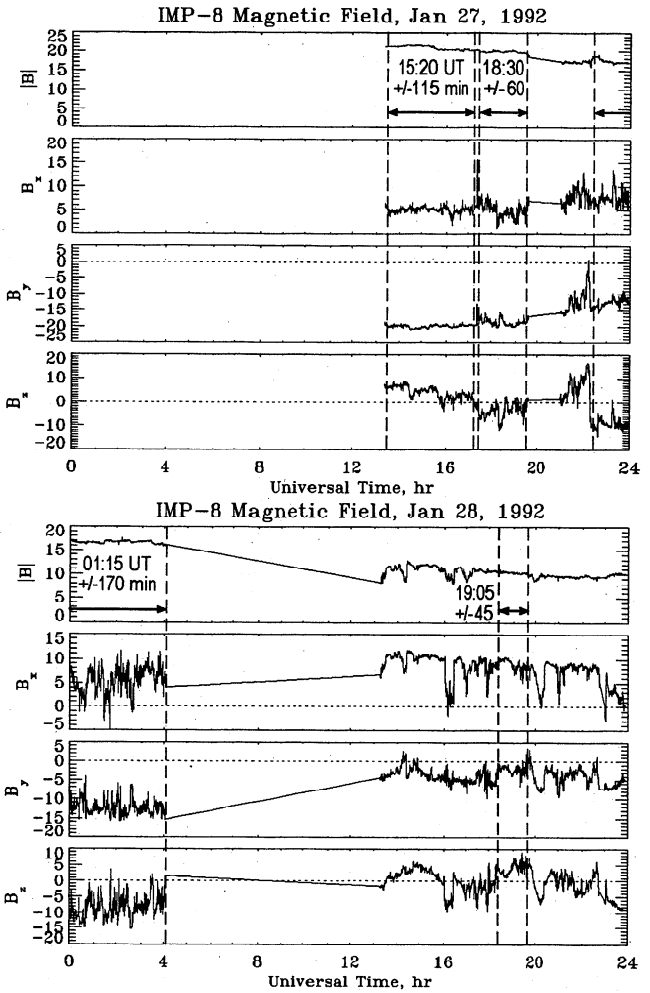

Figure 1. Time history of the IMF as observed by IMP 8 during the January 1992 GEM campaign. Mapping of the field-aligned currents and cross-polar cap potential and the separatrix are present in the following for the three periods around 1520 and 18:30 on January 27, and 01:15 January 28. A fourth period around 1905 on January 28 was discussed by *Lyons et al.* [1996], but the data are too sparse to make a meaningful comparison.

This method works very well for the present case study, since for most of the time, B_x IMF was slowly varying.

3.2. Interval 1: 1520 UT $\pm$ 115 min

The field-aligned currents into the northern and southern hemisphere as inferred by AMIE, the global simulations, and IZMEM are shown in Figure 3. The IMF for this period is characterized by northward IMF with a strong B_y component with $\boldsymbol{B} \simeq (5, -20, 5)$. The images are constructed slightly differently in that AMIE uses all the data over the period to calculate one synoptic map, whereas the simulations average all the 10 minute snapshots to produce an average synoptic map. IZMEM uses a statistical average of archived data that can be used to specify the auroral electrodynamics for the observed IMF conditions. Despite these differences in techniques it is seen that all three models predict a highly distorted current system from the statistical

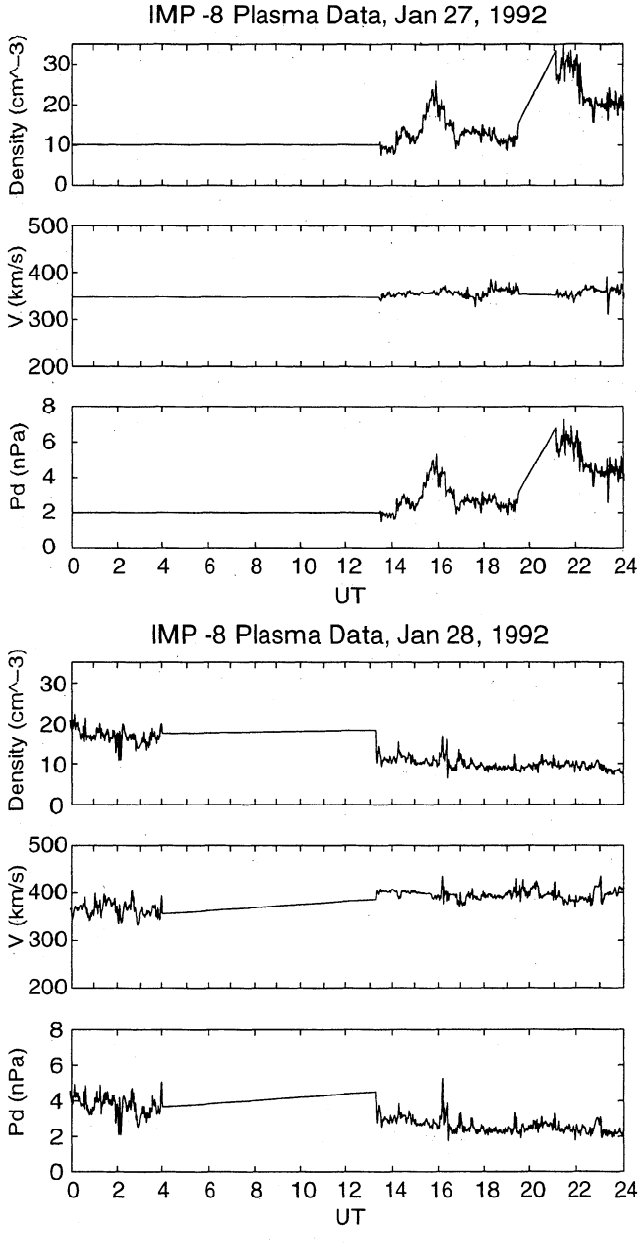

Figure 2. Time histories of the solar wind density, speed, and dynamic pressure corresponding to Figure 1. The solar wind conditions for all but the first interval are approximately steady. The jump in plasma density in the first interval tends to increase the auroral activity in the latter part of the interval.

current maps of *Iijima and Potemra*, [1976, 1978]. This distortion of the field-aligned current system is due to a large negative B_y component of the IMF which forces the reconnection site to be on the dawnside in the northern hemisphere and on the duskside in the southern hemisphere.

For the northern hemisphere in Figure 3 it is seen that there is a pair of upward and downward currents in the postnoon sector (i.e., between 1200 and 1800 MLT) predicted by all three models. For both AMIE and the global simulations the lower-latitude part of the pair extends into the dusk sector and is associated with the region 1 current system. There is also some suggestion of this feature in IZMEM, but the current there is relatively weak. The high-latitude part of the pair is sometimes called the cusp/mantle currents [*Lyons et al.*, 1996]. However, currents in these regions for more typical IMF conditions are also called the northward B_z (NBZ) currents or region 0 currents. We shall use the latter nomenclature in the rest of this paper.

In the southern hemisphere all three models indicate that the dawn region 1 current is much stronger than its dusk counterpart. This current extends well into the nightside. In addition, there is a strong region 0 current near noon.

The magnitudes of the total integrated current into or out of the ionosphere also show some interesting features. The downward integrated current inferred from AMIE is 2.1 MA for the northern hemisphere and 3.1 MA for the southern hemisphere. The corresponding values from the global simulations are in good agreement at 2.2 MA and 3.0 MA, respectively. The total current predicted by IZMEM is about the same, but it is fractionally smaller in the northern hemisphere at 1.2 MA and fractionally higher in the southern hemisphere at 4.0 MA.

The fact that the upward and downward currents are in approximate balance implies that for this interval the noon region 0 currents are actually providing the return path for the region 1 currents. This result is intriguing, since, will be as discussed below, the region 1 currents, particularly those of the dayside, appear to be on closed field lines, while the region 0 currents appear to be on open field lines. As such, the current path can be very complicated.

The position of the separatrix between open and closed field lines can be exactly determined in the simulations by using field line tracing. However, experimentally, the separatrix has to be inferred from particle properties. One method is to identify specific populations (e.g., soft electron precipitation [*Lyons et al.*, 1996]) that are associated with open or closed field lines. However, this proxy for the separatrix depends on the energy of the particles involved. A second proxy that is sometimes used is the position of the flow reversal in the polar cap. This convective flow follows the contours of potential for convection dominated by $\boldsymbol{E} \times \boldsymbol{B}$ drifts and would therefore be associated with the saddle point in the polar cap potential map. This proxy is only approximate, particularly during northward IMF, when the polar cap shrinks and possibly pulls away from the position of the region 1 currents with the development of intense currents in the polar cap.

Note that the definition of "open" and "closed" is slightly different in these different methods. For field line tracing, "closed" means that the field line returns to Earth whereas "open" means that one end of the field line does not return to Earth over the region in which the field-line tracing is made. In the simulations, magnetotail field lines can run parallel to the plasma sheet

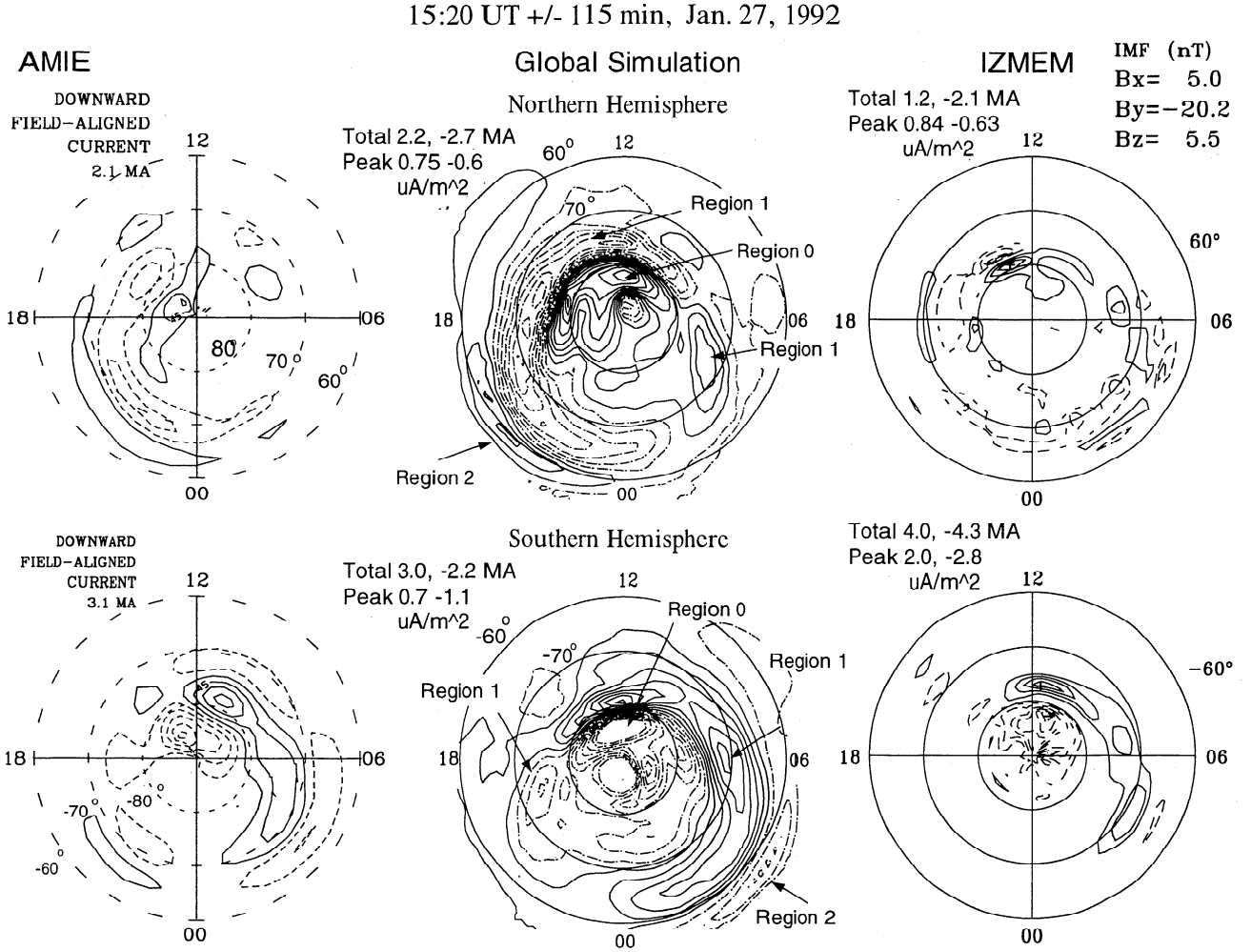

Figure 3. The field-aligned currents as predicted by AMIE, global simulations, and IZMEM. The solid contours indicate currents along the magnetic field, and the dashed contours indicate currents that are antiparallel to the magnetic field. The position of the region 0, 1, and 2 currents and their relative intensity for both hemispheres are in good agreement. The asymmetry and the strong region 0 currents are due to strong negative B_y and northward B_z components in the IMF. The magnitude of the currents inferred from AMIE and the global simulations are in good agreement, while IZMEM tends to be fractionally lower.

for long distances before eventually threading through the distant tail current sheet. These field lines do not necessarily return to Earth, but the particle populations on them would be consistent with the definition of "closed" from the particle perspective. As a result the magnetic definition would indicate that the field line is open but from the particle definition it would be closed. In other words, the latitude determined by the modeling definition of "open," particularly in the tail, should be considered a lower limit relative to the particle boundaries that are used to determine "open."

Figure 4 shows the positions of the separatrix identified by AMIE and the global modeling. On the dayside the soft electron zone sets the limits for the separatrix, and the cusp/mantle precipitation coincides with the region 0 currents. Near noon the separatrix lies at approximately 75°, while near midnight it lies at about 70°. On the dawn and dusk sectors the AMIE results show some uncertainty, lying between 70° and 80°.

For comparison, the right-hand side of Figure 4 shows the global modeling results at three different times during the observing period. The asymmetry seen in the field-aligned currents is also seen in the position of the separatrix, with the dawnside being more open than the duskside in the northern hemisphere, while the reverse is true in the southern hemisphere. At the earliest time the polar cap size is the smallest with the noon separatrix sitting at 80° and the nightside separatrix sitting at 68°.

At later times the oval is seen to expand in all directions by about 2° to 3° in magnetic latitude. This increase coincides with B_z IMF becoming less northward and the dynamic pressure increasing to about 5 nPa. It is seen that the limits of the separatrix essentially span the region identified by AMIE, particularly on the dayside. The main difference is that the night-

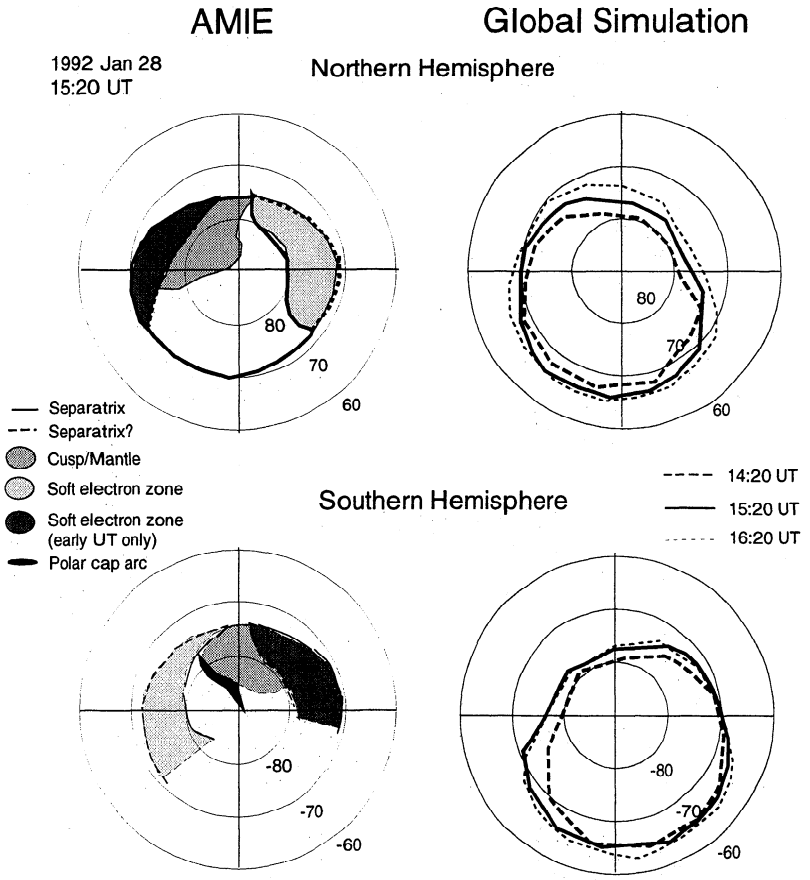

Figure 4. Position of the separatrix as determined by AMIE using DMSP particle data and by the global modeling using field line mapping. The dayside position is in good agreement with the global modeling showing some expansion as the solar wind dynamic pressure increases and the northward B_z decreases at late times. In the nightside the global modeling indicates that the separatrix appears a few degrees lower in latitude than the particle signatures used by AMIE.

side separatrix in the model appears systematically at lower latitudes than those identified by AMIE. As discussed above, this difference is primarily attributed to the definition of "open" as identified by particles and magnetic field modeling.

The final diagnostic is the cross-polar cap potential. Again some caution is required here because AMIE calculates the actual ionospheric potential with the aid of an assumed ionospheric conductivity. As described in section 2, to minimize confusion from boundary conditions the global model calculates the magnetospheric potential and maps the potential near the inner boundary down into the ionosphere. The comparison between AMIE and the global model potentials is shown in Figure 5. The main feature common to both is the position of the strongest electric fields, i.e., where the contours of the potential are most closely spaced. These regions of enhanced convection occur on the duskside in the northern hemisphere and on dawnside in the southern hemisphere at around 80°. The position of the saddle point in the potential is in approximate agreement between the two models and with the position determined by the magnetic field mapping in Figure 4.

However, there are substantial areas of disagreement: (1) the model shows more convection near noon in the northern hemisphere at mid-latitudes, (2) the model potentials are 2 to 4 times larger than predicted by AMIE, and (3) AMIE predicts a very large (30 kV) difference in potential between the northern and southern hemisphere, which is of the order of the total cross-polar cap potential, while the global model predicts only a 10 kV difference, which represents only a 7% difference in potential. If the difference in potentials were real, then the difference in polar cap size would be huge. However, the above results show that this is not the case and that the global model is sensitive to changes in polar cap size as the IMF conditions vary. Indeed the main difference between AMIE and the global modeling is that in the simulations the dominant dusk (dawn) cell in the northern (southern) hemisphere extents to mid-latitudes on the dayside, whereas the AMIE potential pattern is limited to sub-auroral latitudes. In the global model the midlatitudes add about 50-60 kV to the total magnetospheric potential.

As an independent check on the cross-polar cap potential, comparisons were made with the IZMEM and Weimer empirical models. The predictions for these models are shown in Figure 6. While the actual shape of the convection cells predicted by IZMEM differs for the northern hemisphere from those in Figure 5, the

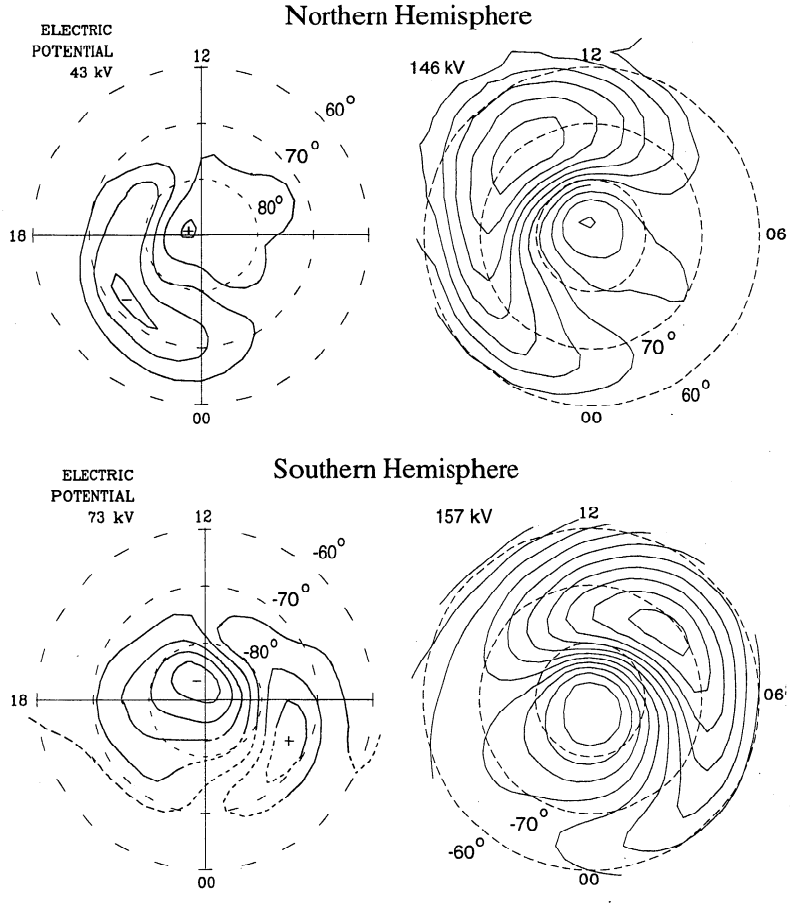

Figure 5. Cross-polar cap potential corresponding to Figure 4. The position of the strongest convection (i.e., most closely spaced contours) and the position of the separatrix as determined from the saddle point of the potentials are in good agreement. However, the magnitude of the potential from the global modeling is much larger as a result of the convection in the dayside at midlatitudes.

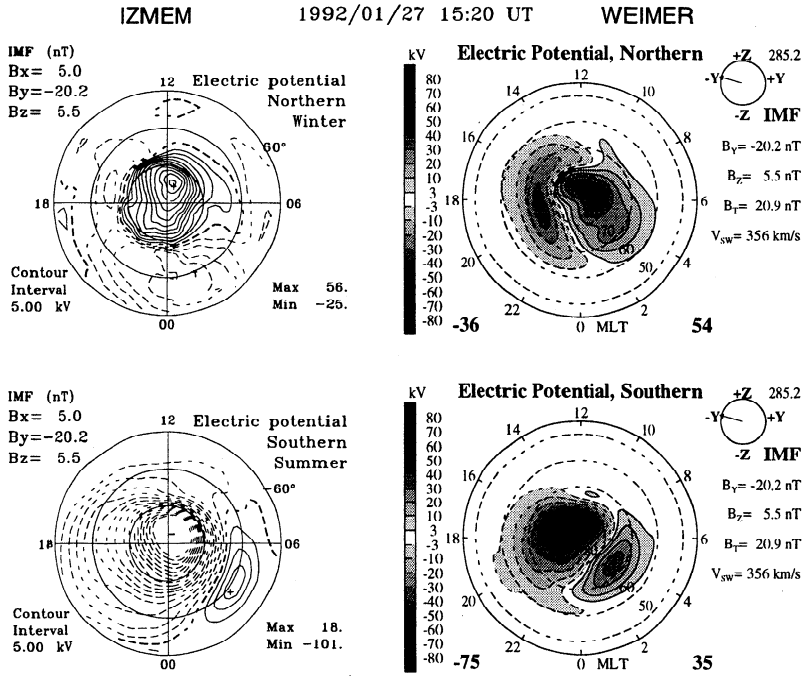

Figure 6. Potential pattern predicted by the IZMEM and Weimer empirical models. The presence of a distorted two-cell pattern is seen in both models. The potentials higher the AMIE results.

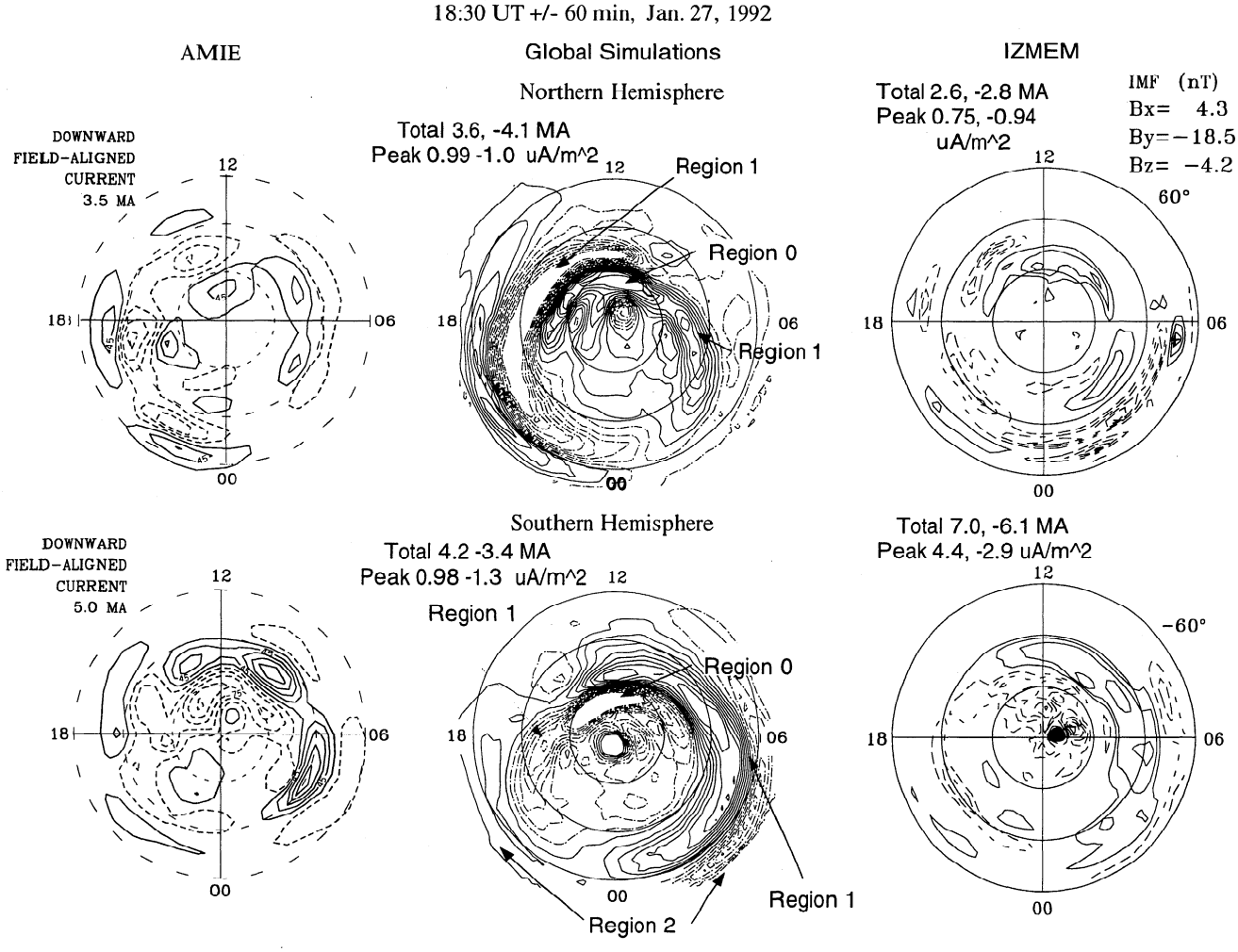

Figure 7. Comparison of the field-aligned currents for the second interval. Both AMIE and the global simulations show an intensification of the region 1 currents by nearly 60% over that shown in Figure 3. IZMEM also indicates a similar increase in the southern hemisphere, while the northern hemisphere does not show any significant increase.

position of the strongest convection is similar in that it extends from about 11 MLT, all the way around the duskside, to about 0200 MLT. The southern pattern is very similar to the ones in Figure 4, particularly the AMIE pattern. However, the predicted magnitudes of the potentials lie close to the global model results with 81 and 119 kV for the northern and southern hemispheres, respectively. These potentials are dominated by the B_y component of the IMF, and changing the B_z by 1-2 nT to cover the variability in the IMF does not change the predicted ionospheric potential by more than a few kV.

The Weimer potential patterns show the presence of two strong cells in both hemispheres. This result raises the possibly that the polar cap cell in the northern hemisphere inferred by AMIE may not be completely resolved. The shapes of the potentials are similar to the simulation results except that the latter show more convection at middle to low latitudes on the dayside. The Weimer potentials are again higher than the AMIE results at 90 and 110 kV and lie very close those inferred from IZMEM.

3.3. Interval 2: 1830 UT ±0 60 min

The B_x and B_y for this period are approximately the same as those in the first interval, but B_z is now southward at about -3 nT. The predicted field-aligned current from AMIE, global simulations and IZMEM are shown in Figure 7. All three models show that the region 0 currents remain relatively strong. Both AMIE and the global simulations show that the region 1 and region 2 currents on both the dawn and dusk flanks are enhanced, relative to the northward IMF case in the previous section, but the dusk (dawn) region 1 current in the northern (southern) hemisphere starts to become the dominant current system. IZMEM also shows this enhancement of the region 1 current in the southern hemisphere, but it is less clear in the northern hemisphere. The latitudinal and MLT variations predicted by the global modeling are seen to closely match those

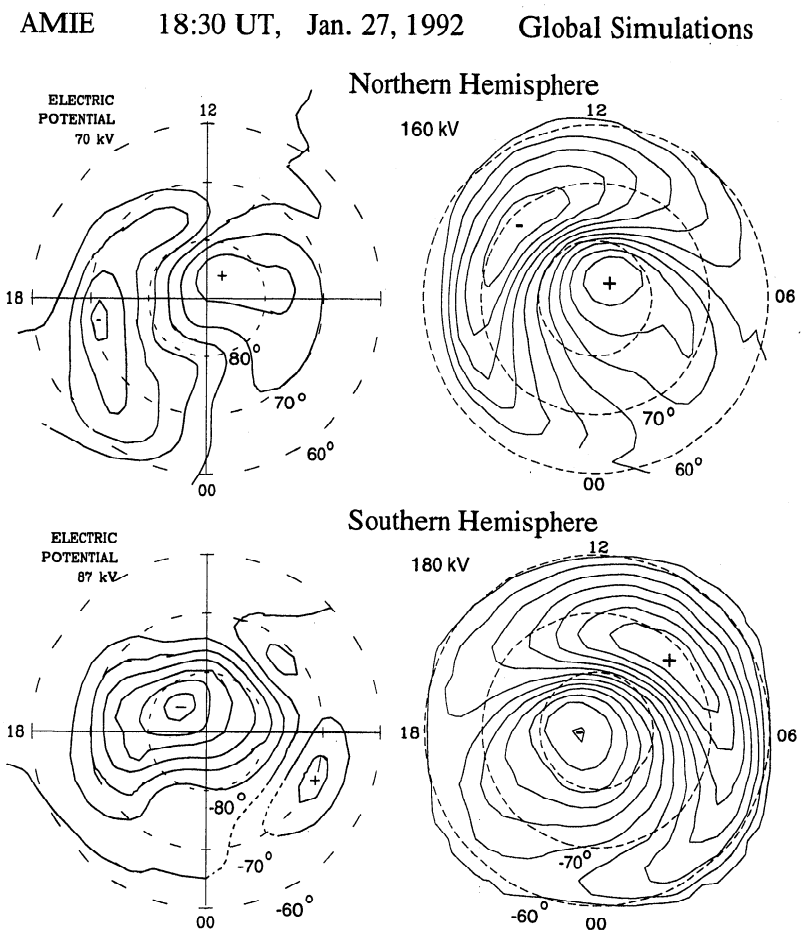

Figure 8. AMIE and global simulation predictions for the cross-polar cap potential for the second interval. The potential is seen to increase, but the simulations again show a strong component at lower to middle latitudes, which raises the predicted potential above that of AMIE. A distorted two-cell pattern persists as a result of due to the strong negative B_y in the IMF.

inferred from AMIE and IZMEM for the southern hemisphere. The magnitude of the increase in the total integrated current is approximately 40-60% for AMIE and the global models and fractionally higher at 80-100% for IZMEM.

Because of the enhancement of the region 1 currents the configuration more closely resembles the statistical current patterns of *Potemra* [1994]. In particular, in the northern hemisphere the dawn region 1 current attaches smoothly to the dusk region 0 current, while in the southern hemisphere the dusk region 1 current attaches to the dawn region 0 current.

The separatrix as identified by magnetic field mapping for the global modeling and the particle data for the AMIE results lie close to the saddle points of the potential maps, so that only the latter are shown in Figure 8. It is seen that the global modeling predicts a distorted two-cell pattern where the dusk (dawn) cell in the northern (southern) hemisphere is centered at 70° and the dawn (dusk) cell is again in the polar cap at about 85°. These latitudinal positions are consistent with AMIE.

There are some differences in the local time positions. In the southern hemisphere the global modeling shows the polar cap cell being centered at 1800 MLT whereas AMIE indicates a center closer to 1500 MLT. However, this difference is not that significant in that it represents the region of smallest convection. More important, the position of the saddle point or separatrix is in reasonable agreement between the two models, as is the position of the strongest convection over the polar cap.

The global model still shows enhanced convection on the dayside at midlatitudes that is not incorporated in AMIE. As a result the global model results remain relatively high, nearly a factor of 2 higher than AMIE. However, both show the same trend in that the cross-polar cap potential is predicted to increase as a result of the southward turning of the IMF. AMIE indicates changes of 14 to 37 kV, while the global modeling indicates changes of 16 to 23 kV.

The corresponding potential maps from IZMEM and Weimer empirical models are shown in Figure 9. The IZMEM potentials incorporate much of the same features as the AMIE potentials, including the latitude

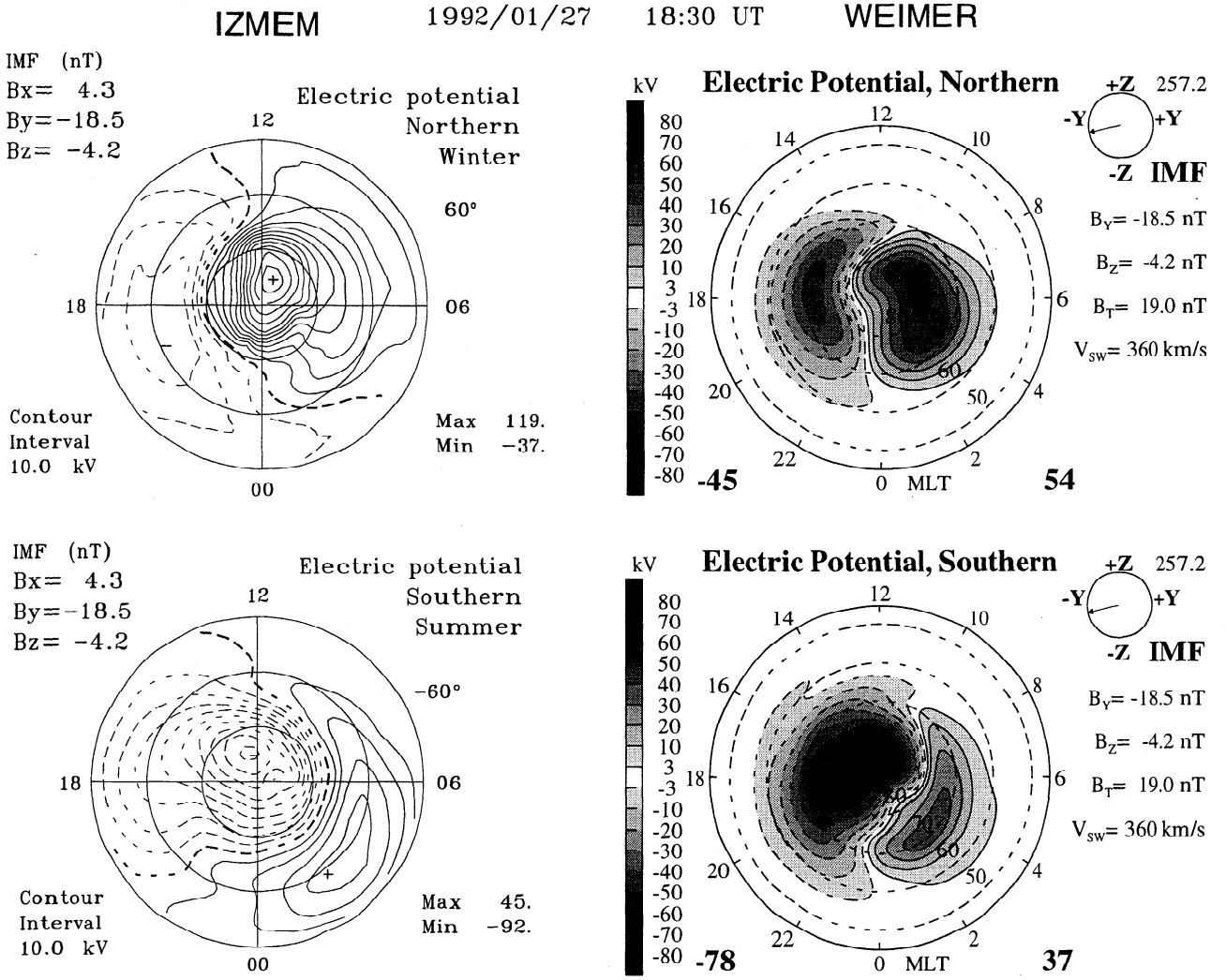

Figure 9. Corresponding potentials predicted by IZMEM and the Weimer empirical model for the period in Figure 8. These models also show a distorted two-cell pattern with potentials 20-40% above the AMIE result.

and MLT position of the two cells in both the northern and southern hemispheres. However, the total potential drop is much larger at 156 kV for the northern hemisphere and 137 kV for the southern hemisphere. There is about a ±10 kV range in the potential for ±1 nT variations in B_z IMF. The higher potential is also associated with convection extending down to the lower latitudes.

The Weimer model also shows an elevated potential relative to the first interval, increasing from 90 to 99 kV in the northern hemisphere and from 110 to 115 kV in the southern hemisphere. The distorted two-cell pattern is very similar to that seen in the other models, the main difference being that the global simulations again appear to include a low- to middle-latitude component on the dayside, which raises its potential above the other models. The position of the separatrix from the Weimer model is at about 70°-75° near noon and at about 65°-70° near midnight, consistent with the simulations. This result suggests that the shape of the auroral oval and hence the polar cap potential are consistent between models and that the main difference in the magnitude is due to the components used to calculate the potential.

3.4. Interval 3: 0115 UT ± 170 min

In the last period, B_y IMF has declined substantially to -12.9 nT, and B_z IMF is strongly southward at about -8.9 nT. The corresponding AMIE, global simulation, and IZMEM predictions for the field-aligned currents are shown in Figure 10. Because this interval is for several hours, effects from the northward proceeding IMF, particularly the region 0 currents, are relatively weak. Nevertheless, they are still present, and the dawn region 1 currents remain attached to the dusk region 0 currents in the northern hemisphere in all three models as in the other periods. For the southern hemisphere the dawn region 1 current is the dominant current in all three models, although the global simulations show it at about 2° lower than the other models.

All three models show increases in the total integrated field-aligned currents. Most of the increase comes

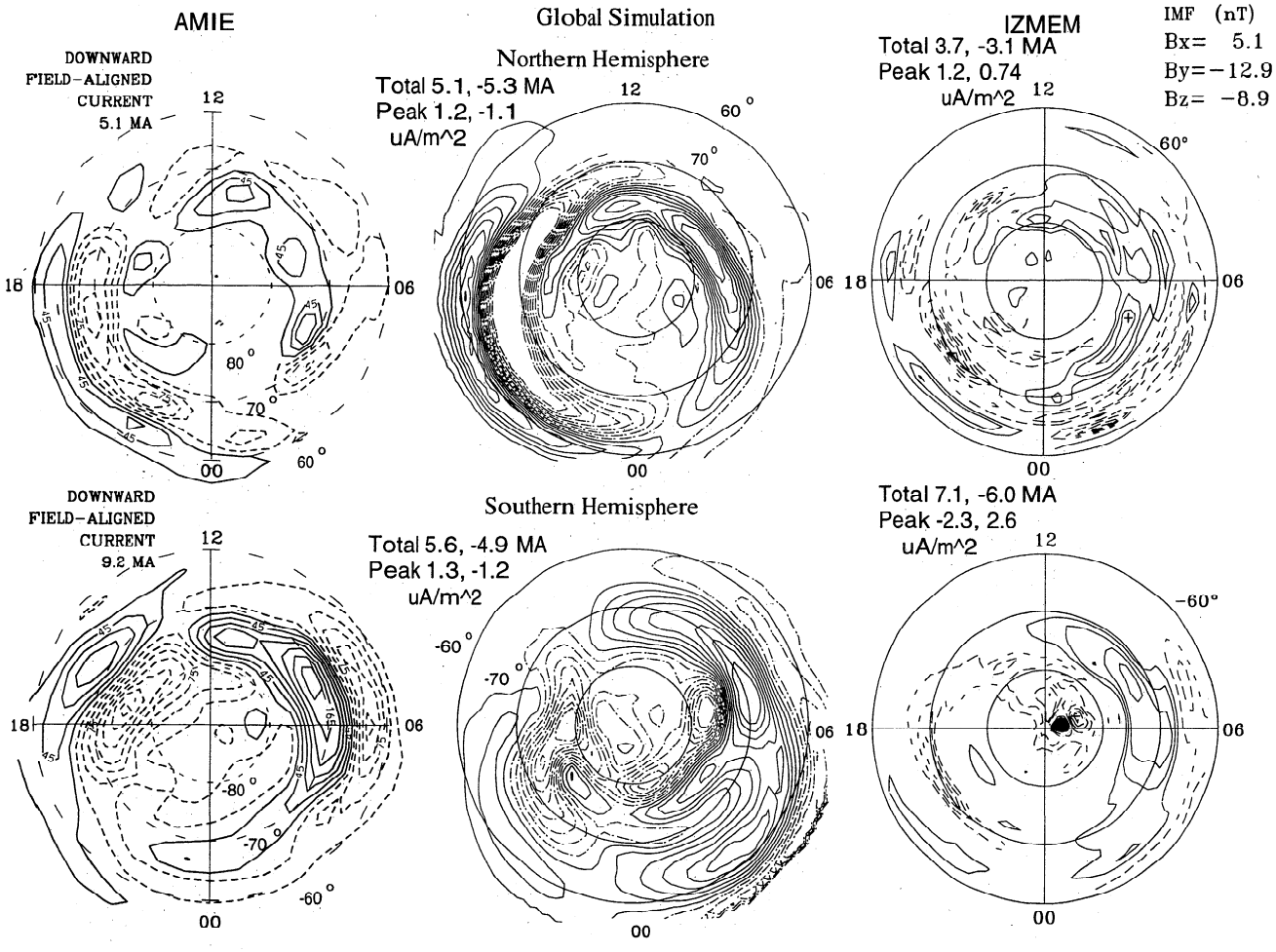

Figure 10. Comparison of the field-aligned currents for the third interval. There is a further intensification of the region 1 and 2 currents and a decline in the region 0 currents predicted by AMIE and the global simulations in association with the IMF becoming more southward.

from an increase in the area of the currents rather than an increase in the peak current density. In other words, the peak current density appears to reach saturation, and the oval expands to sustain the total amount of current demand for the magnetospheric dynamics. There is again good agreement with total current into the northern hemisphere, but AMIE predicts about twice the total current in the southern hemisphere. This latter current is also larger than that predicted by IZMEM.

As discussed above, the intensification of the field-aligned currents is associated with a significant increase in the size of the polar cap. This result is illustrated in Figure 11, which shows the positions of open field lines as determined by AMIE using observed particle properties and by the global modeling through field line mapping. In relation to Figure 4 it is seen that the dayside portion of the auroral oval has on average moved equatorward by 3°-5° in both models. There is still some dawn-dusk asymmetry in the global model due to the presence of the negative B_y in the IMF. However, the asymmetry is smaller than that in Figure 4, in line with the reduction in the magnitude of B_y IMF.

The results for the nightside oval are less in agreement with AMIE, indicating that the average oval is at about 72° near midnight for both hemispheres. This position is essentially unchanged from the northward IMF case in Figure 4. The global modeling predicts higher variability in association with substorm activity, but the nightside oval in general lies below 70°.

The position of the saddle points in the potential maps in Figure 12 for the two models approximately coincides with the position of the open field lines as determined from the field line mapping in Figure 11. The particle boundaries of Figure 11 lie poleward of this position, particularly in the nightside. This result may indicate that the particle boundaries may be representative of the poleward edge of the auroral oval, whereas the mapping may be indicative of the equatorward edge.

The shape of the potential predicted by the global modeling, as in the other two intervals, agrees well with the shapes inferred by AMIE in both local time and latitude for both hemispheres. The only major difference in the present case is an intrusive feature near dawn in the southern hemisphere in the global modeling. How-

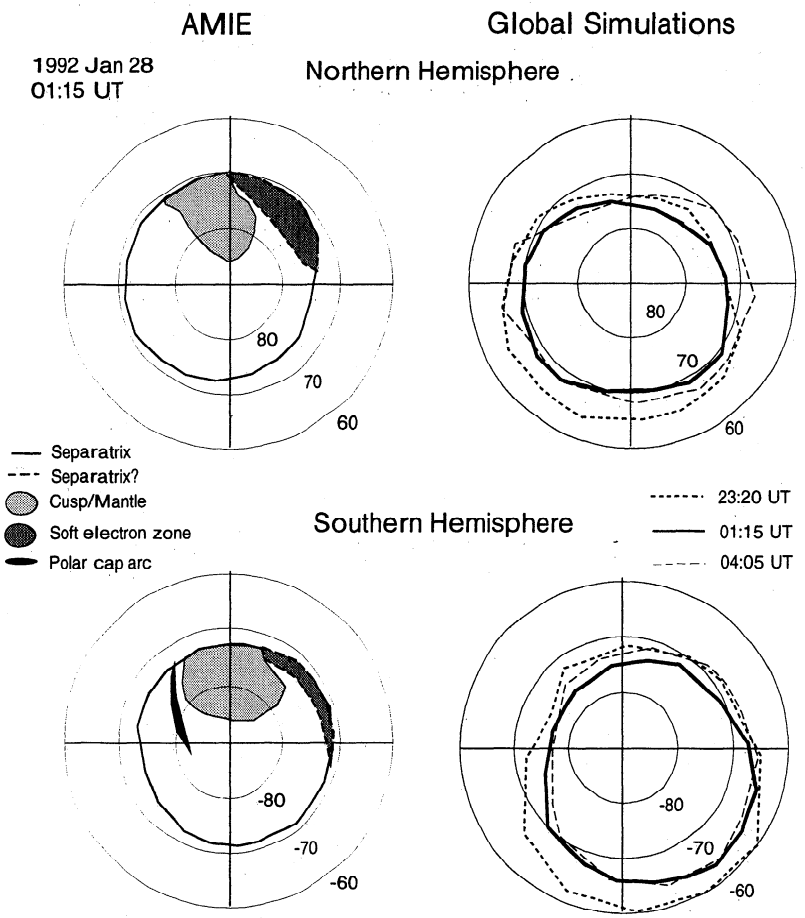

Figure 11. Position of the open and closed field lines as determined from AMIE using particle data and the global simulations using magnetic field mapping. The results are in reasonable agreement on the dayside. However, on the nightside the AMIE results are in essentially the same position as those for the northward IMF case in Figure 4. On the other hand, the simulations show a highly variable position due to substorm activity, but on average at a position lower than that suggested by AMIE.

ever, this intrusion is in fact seen in both the IZMEM and Weimer models, as shown in Figure 13.

The magnitudes for the potential are similar to the potentials in the previous interval with AMIE predicting potentials of the order of 90 kV and the global simulations potentials of 170 and 150 kV. The IZMEM model indicates comparable potentials at 172 and 142 kV, while Weimer indicated intermediate potentials at 118 and 116 kV, respectively. The models that indicate the higher potentials, i.e. the global simulations and IZMEM, do so because they appear to include lower-latitude convection.

4. Summary and Discussion

The above results show that there is a significant disparity in the magnitude of the cross-polar cap potential predicted by the different models. Nevertheless, the difference between the models is systematic and can be very informative. The AMIE method predicts the lowest potential, followed by the Weimer model, IZMEM, and the global modeling simulations. The typical factor between highest and lowest is between about 1.5 and 3. Despite this range in magnitudes the difference in potentials as one moves from the relatively quiet times in the first interval to the more active times associated with southward IMF in the last two intervals is about the same for each model. In particular, AMIE, Weimer, and the global modeling predict changes of about 30 kV in the potential. IZMEM also predicts changes of the order of 30 kV for the southern hemisphere, but for the northern hemisphere the change is nearly 90 kV. The point is that the different models appear to be able to differentiate changes in the convection patterns, even though the absolute magnitude of the cross-polar cap potential is uncertain. The higher potentials of the simulations are not unique to the present simulations. The results from the global MHD models of *Raeder* [1997] and *Slinker et al.* [1997] give potentials 10-30 kV higher than the results presented here.

The higher results of the present global model are due to two additional factors. First, the global modeling produces a magnetospheric potential, which is mapped onto the ionosphere. As such, field-aligned potential drops that occur between the inner boundary of the simulations and the true ionosphere are neglected. Such

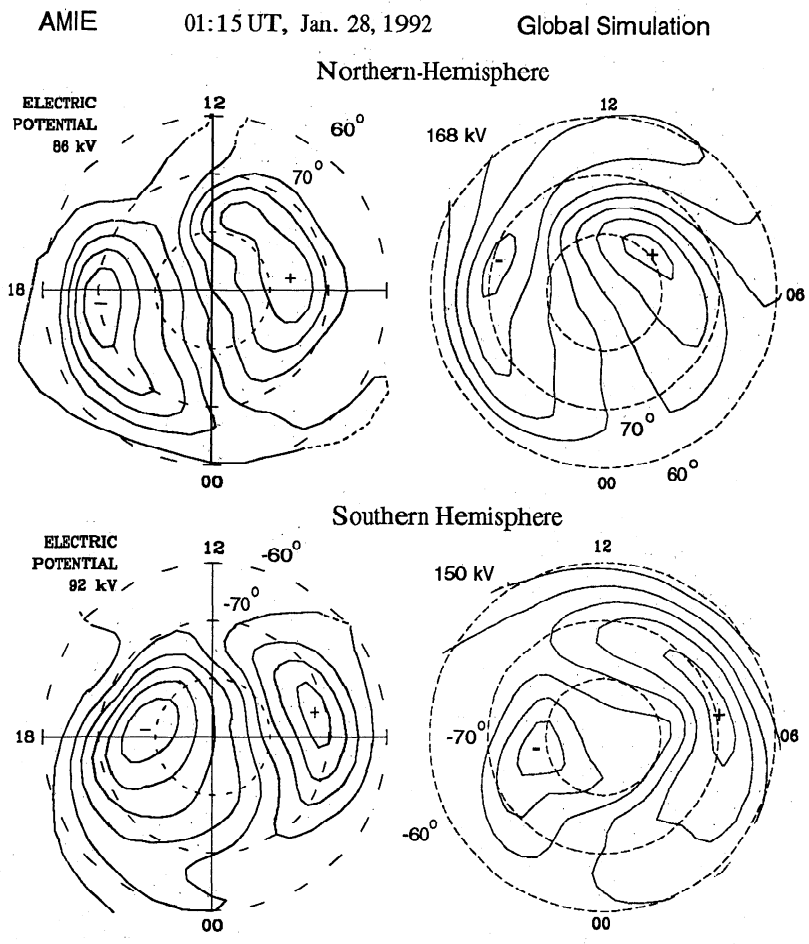

Figure 12. Potential maps corresponding to Figure 10. The position of the saddle point in the potentials is consistent with the magnetic field mapping in Figure 11. Strong dayside convection continues to keep the simulation potential above the AMIE potential.

potential drops could account for differences of several kV, possibly up to 10-20 kV during active periods when B_z IMF is very negative. A second factor is that the global modeling predicts significant convection at mid-latitudes driven by the growth of the dusk (dawn) cell in the northern (southern) hemisphere that is produced by the large B_y component in the IMF. This convection cell adds an additional 50-60 kV to the simulation potentials. This component seems to have the strongest relative contribution during northward IMF, when the polar cap potential is relatively small, and is less important during active periods.

While the above difference is a concern, all four models appeared to be consistent in their ability to predict the regions of strongest convection and the position of the separatrix. The main difference between models was with IZMEM, which predicts that the polar cap cell for the winter hemisphere should be almost centered on the magnetic pole for the conditions studied here. The agreement between models on these key features indicates that the above differences in potential may be due to modeling assumptions at middle to low latitudes.

The inferred current patterns from AMIE, IZMEM, and the global simulations are in reasonable agreement. The total integrated current for the northern hemisphere is also in agreement, but AMIE and IZMEM tend to predict substantially higher currents in the southern hemisphere than in the northern hemisphere. However, it should be noted that the coverage of the southern hemisphere is less than that of the northern hemisphere, and hence the results for the southern hemisphere could be subject to more error.

The main results of this paper are as follows:

1. The field-aligned currents into the auroral regions are very sensitive to changes in B_z IMF, with changes of the order of 250% occurring in the above case studies.

2. The cross-polar cap potential over the same cases changes by only about 25-50% in the different models. This result may be counterintuitive, but as the convection pattern changes the magnetospheric configuration also changes, causing a redistribution of current throughout the magnetosphere and the auroral ova, including local time and latitudinal variations. Thus the assumption that the potential is directionally proportional to the current appears to be an oversimplification of the problem.

3. When the IMF is dominated by B_y with a north-

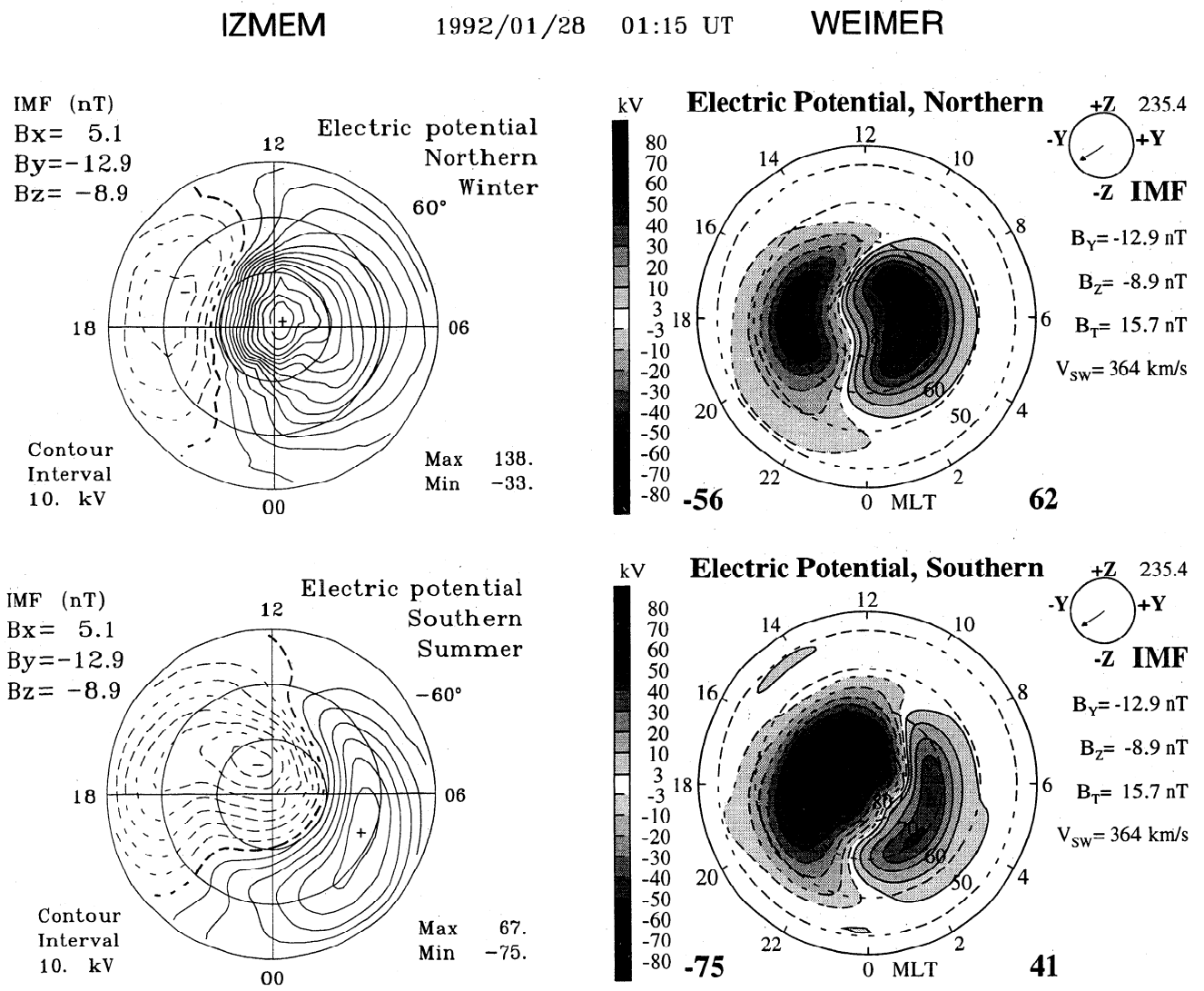

Figure 13. Corresponding potentials from IZMEM and the Weimer empirical model. The potentials have intensifiedin relation to the previous periods as a result of the strong southward IMF present. IZMEM shows the largest increase, which is associated with convection at midlatitudes in conjunction with enhanced convection over the polar cap.

ward B_z component, the field-aligned current system can be highly distorted from the statistical pattern of *Iijima and Potemra* [1976, 1978] with the cusp or region 0 current sufficiently strong to provide the return current for the region 1 currents.

4. The current density appears to be limited to a few $\mu A/m^2$, and much of the increase in current in the most active period comes from an increase in area rather than in intensity.

5. AMIE, IZMEM, and the global simulations all show the attachment of the region 1 and 0 currents for nonzero B_y IMF as discussed by *Potemra* [1994].

6. The B_y IMF component also produces an asymmetry in the auroral oval with the dawnside being smaller in the northern hemisphere for negative B_y.

The question of the position of the separatrix in relation to the above currents remains very interesting. The region 0 currents are clearly on open field lines in both the AMIE and global simulation results. The dayside region 1 currents in both models appear on closed field lines. In the nightside there is some ambiguity concerning the relative position of the region 1 currents. If one uses the particle signatures to define the position of the separatrix, then the region 1 currents are in the closed region. However, if one uses either the saddle point in the potential maps or the mapping of magnetic field lines, then the separatrix appears about 3°-5° lower in latitude, in which case the region 1 currents are spread over both open and closed field lines. It is possible that the particle boundary may indicate the poleward edge of the auroral oval and the saddle points in potential or current may be related to the equatorward edge. The separatrix in the modeling is sensitive to local activity, moving by as much as a few degrees during the individual case studies, even though the IMF was approximately steady.

Acknowledgments. This work was supported by NSF grant ATM-9321665 and NASA grant NAGW-5047 to the University of Washington, NSF grant ATM-9506169 to Mission Research Corporation, and NSF grants OPP-9318766 and ATM-9523329 to the University of Michigan. The simulations were supported by the Cray C-90 at the San Diego Supercomputing Center, which is supported by the NSF. The authors would like to thank L. R. Lyons and G. Lu allowing access to the AMIE data and to the Geospace Environment Modeling (GEM) program, supported by NSF, that provided the umbrella for the collection and analysis of the data used in here.

The Editor thanks G. L. Siscoe and another referee for their assistance in evaluating this paper.

References

Boris, J. A., and D. L. Book, Flux-corrected transport, 1, SHAST:, A fluid transport algorithm that works, *J. Comput.l Phys., 11*, 38, 1973.

Cattell, C. A., F. S. Mozer, Substorm electric fields in the earth's magnetotail, in *Magnetic Reconnection in Space and Laboratory Plasmas, Geophys. Monogr. Ser.*, vol. 30, edited by E. W. Hones Jr., AGU, Washington, D. C., 1984.

Dongsu, R., T. W. Jones, and A. Frank, Numerical magnetohydrodynamics in astrophysics: Algorithm and tests for multidimensional flow, *Astrophys. J., 452*, 785, 1995.

Fedder, J. A., S. P. Slinker, J. G. Lyon, and R. D. Elphinstone, Global numerical simulation of the growth phase and the expansion onset for a substorm observed by Viking, *J. Geophys. Res., 100*, 19,083, 1995.

Iijima, T., and T. A. Potemra, The amplitude of field-aligned currents at northern high latitudes observed by Triad, *J. Geophys. Res., 81*, 2165, 1976.

Iijima, T., and T. A. Potemra, Large-scale characteristics of field-aligned currents associated with substorms, *J. Geophys. Res., 83*, 599, 1978.

Krall, N. A., and A. W. Trivelpiece, *Principles of Plasma Physics*, San Francisco Press, San Francisco, 1986.

Lu, G., et al., Characteristics of ionospheric convection and field-aligned current in the dayside cusp region, *J. Geophys. Res., 100*, 11,845, 1995.

Lyons, L. R., G. Lu, O. de la Beaujardière, and F. J. Rich, Synoptic maps of polar caps for stable interplanetary magnetic field intervals during January 1992 geospace environment modeling campaign, *J. Geophys. Res., 101*, 27,283, 1996.

Ogino, T., R. J. Walker, and M. Ashour-Abdalla, A global magnetospheric simulation of the response of magnetosphere to a northward turning of the interplanetary magnetic field, *J. Geophys. Res., 99*, 11,027, 1994.

Papitashvili, V. O., B. A. Belov, D. S. Faermark, Y. I. Feldstein, S. A. Golyshev, L. I. Gromova, and A. E. Levitin, Electric potential patterns in the northern and southern polar regions parameterized by the interplanetary magnetic field, *J. Geophys. Res., 99*, 13,251, 1994.

Papitashvili, V. O., C. R. Clauer, A. E. Levitin, and B. A. Belov, Relationship between the observed and modeled modulation of the dayside ionospheric convection by the IMF B_y component, *J. Geophys. Res., 100*, 7715, 1995.

Potemra, T. A., Sources of large-scale Birkeland currents, in *Physical Signatures of Magnetospheric Boundary Layer Processes*, edited by J. A. Holtet and A. Egeland, p. 3., Kluwer Acad., Norwell, Mass., 1994.

Raeder, J., Comparison of MHD results with the Jan. 28, 1992 events, paper presented at the GEM Workshop, organized by H. Spence, Snowmass, Colorado, June 16-20, 1997.

Richmond, A. D., and Y. Kamide, Mapping electrodynamic features of the high-latitude ionosphere from localized observations, Technique, *J. Geophys. Res., 93*, 5741, 1988.

Richtmyer, R. D., and K. W. Morton, *Difference Methods for Initial Value Problems*, p. 300, Interscience, New York, 1967.

Slinker, S., J. Fedder, and J. Lyon, Topological boundaries for the GEM Challenge, paper presented at the GEM Workshop, organized by H. Spence, Snowmass, Colo., June 16-20, 1997.

Weimer, D. R., Models of high-latitude electric potentials derived with a least errors fit of spherical harmonic coefficients, *J. Geophys. Res., 100*, 19,595, 1995.

Weimer, D. R., A flexible, IMF dependent model of high-latitude electric potentials having "space weather" applications, *Geophys. Res. Lett., 23*, 2549, 1996.

Winglee, R. M., Non-MHD influences on the magnetospheric current system, *J. Geophys. Res., 99*, 13,437, 1994.

Winglee, R. M., R. M. Skoug, R. K. Elsen, M. Wilber, R. P. Lin, R. P. Lepping, T. Mukai, S. Kokubun, H. Reme, and T. Sanderson, IMF induced changes to the nightside magnetotail: A comparison between WIND/Geotail/IMP 8 observations and modeling, *Geophys. Res. Lett., 24*, 947, 1997a.

Winglee, R. M., S. Kokubun, R. P. Lin, and R. P. Lepping, Flux rope structures in the magnetotail: Comparison between Wind/Geotail observations and global simulations, *J. Geophys. Res.*, in press, 1997b.

V. O. Papitashvili, Space Physics Research Laboratory, University of Michigan, Ann Arbor, MI 48109. (e-mail:papita@umich.edu)

D. R. Weimer, Mission Research Corporation, 1 Tara Boulevard, Suite 302,, Nashua, NH 03062.(e-mail: dweimer@mrcnh.com)

R. M. Winglee, Geophysics Program, Box 351650, University of Washington, Seattle WA 98195-1650. (e-mail: winglee@geophys.washington.edu)

(Received February 12, 1997; revised August 27, 1997; accepted August 28, 1997.)